HHS Public Access

Author manuscript

Soil Sci Soc Am J. Author manuscript; available in PMC 2018 April 13.

Published in final edited form as:

Soil Sci Soc Am J. 2016 ; 80(3): 613–622. doi:10.2136/sssaj2015.11.0414.

A Fourier-Transform Infrared Study of Biochar Aging in Soils

B. Singh[*],

Faculty of Agriculture and Environment, Univ. of Sydney, Sydney, NSW 2006, Australia

Y. Fang, and

Faculty of Agriculture and Environment, Univ. of Sydney, Sydney, NSW 2006, Australia

C.T. Johnston

Crop, Soil and Environmental Science, Purdue Univ., West Lafayette, IN 47907

Abstract

We used diffuse reflectance Fourier-transform infrared (DR-FTIR) spectroscopy, X-ray diffraction (XRD), and chemical and isotopic analyses to characterize the light fraction of four contrasting soils (control and biocharamended soils) to determine changes in biochar properties after aging. Two Eucalyptus saligna Sm. wood biochars, produced at 450°C (B450) and 550°C (B550), were incubated separately in each of the four soils for up to 12 mo at 20, 40, and 60°C. Total C and isotopic ($\delta^{13}C$) methods were used to quantify the amounts of biochar C and native C mineralized during incubation. The DR-FTIR spectra of the light fraction showed distinct absorption bands representing native soil organic C, biochar C, and mineral constituents present in the soils; the mineral bands were consistent with XRD data of the clay fraction of the four soils. Analysis of the DR-FTIR spectra in the ν(C–H) bands showed that the ratio of the aromatic ν(C–H) bands systematically increased relative to the aliphatic ν(C–H) bands with increasing mineralization of biochar C in the B550 amended soils, and this relationship was unique for each soil type. In contrast, this relationship was not observed for the B450 amended soils that contained a relatively smaller proportion of aromatic C.

Interest in biochar technology has increased tremendously since the discovery of high levels of soil organic matter and available nutrients in the Terra Preta soils of the Brazilian Amazon basin (Glaser et al., 2002). Biochar is a black carbon made from biomass under O_2 – deficient conditions. Because biochar contains condensed aromatic structures, which have greater biogeochemical recalcitrance, it can potentially persist in the soil for a long time (Kuzyakov et al., 2009; Lehmann, 2007; Schmidt and Noack, 2000; Schmidt et al., 2002). Due to the greater presumed stability of biochar C compared with much of the organic soil C, biochar has been promoted as a soil amendment to increase soil C sequestration and provide other benefits, such as reducing soil greenhouse gas emissions, enhancing agricultural productivity, and improving soil properties. In addition to increasing the

[*]Corresponding author (Balwant.singh@sydney.edu.au).

SUPPLEMENTAL MATERIAL

The following supplemental material is available online: FTIR band assignments for the two biochars, native soil organic C, and minerals in the light fraction of the biochar-amended soils (Supplemental Table S1), and additional experimental details regarding the ratio of the total C–H stretching intensity of aromatic and aliphatic bands in the FTIR spectra of the light fractions (Supplemental Table S2).

proportion of stable C in the soil, biochar has the potential to reduce greenhouse gas emissions, improve soil properties, enhance agricultural productivity, and reduce the availability of heavy metals in soil (Kookana et al., 2011; Laird et al., 2008; Lehmann, 2007; Namgay et al., 2010; Singh et al., 2010b). The actual stability of biochar amended to soils, however, remains an open question and may vary considerably in different soil types and environmental conditions (Fang et al., 2014a, 2014b).

The structural "backbone" of biochar is a network of condensed aromatic structures that form clusters as thermal pyrolysis (i.e., heating in a reduced O_2 atmosphere) proceeds (Preston and Schmidt 2006). Depending on the C source, pyrolysis temperature, and the amount of O_2 present, a broad spectrum of more easily degradable aliphatic structures and O-containing functional groups may also be present (Fuertes et al., 2010; Gaskin et al., 2008; Kookana et al., 2011; McBeath and Smernik, 2009; Nguyen et al., 2010; Singh et al., 2010a). Furthermore, soil environmental conditions determine the stability of biochar in soils. For example, high soil temperature and moisture conditions have been shown to facilitate the rapid abiotic and biotic oxidation of biochar in soils (Cheng et al., 2006, 2008). Conversely, the interaction of biochar with clay minerals in soils and the consequent entrapment within newly formed aggregates may increase the stability and longevity of biochar in soils (Brodowski et al., 2005b; Fang et al., 2014a, 2014b; Glaser et al., 2000; Keith et al., 2011).

Biochar stability in soils is usually determined by measuring the CO_2 evolved from the biochar-amended soils in conjunction with isotopic techniques (Keith et al., 2011; Zimmerman, 2010). Black carbon, consisting of a range of C products including biochar, char, charcoal, graphite, ash, and soot in soils, has been quantified using a variety of chemical, thermal, photo-oxidation, and spectroscopic procedures (Bornemann et al., 2008; Brodowski et al., 2005a; Schmidt et al., 2001; Skjemstad et al., 2002). Spectroscopic techniques including solid-state ^{13}C nuclear magnetic resonance (NMR) spectroscopy, X-ray photoelectron spectroscopy, and Fourier-transform infrared (FTIR) spectroscopy (Baldock and Smernik, 2002; Cheng et al., 2006, 2008; Mikutta et al., 2009; Rumpel et al., 2001) have been widely used for characterization and monitoring of biochar and organic matter in soils. For example, Baldock et al. (1997) used solid-state ^{13}C NMR spectroscopy to evaluate changes in the chemical structure of organic materials in a range of substrates such as forest litter, peats, composts, and organic and mineral soil horizons. Recently, McBeath and Smernik (2009) modified the ^{13}C NMR method by adsorbing benzene to the black carbon to measure the relative aromatic condensation in the black carbon. Nuclear magnetic resonance spectroscopy remains the preferred laboratory technique for the structural characterization of C in black carbon and biochar because of its ability to distinguish different C nuclei. However, this method is relatively expensive and time consuming (hours per sample), and the required equipment is not available in many research laboratories. In addition, NMR of soil materials requires significant invasive sample pretreatment to remove commonly occurring paramagnetic and ferromagnetic impurities (Hedges et al., 2000).

Fewer studies have used FTIR spectroscopy for the characterization of aged biochars in soils in conjunction with other spectroscopic methods (Cheng et al., 2006; Hilscher and Knicker, 2011; Nguyen and Lehmann, 2009). Cheng et al. (2006) observed an increased intensity of

carboxylic and aromatic bands and a decreased intensity of the aliphatic band in the FTIR spectra of biochar isolated from a soil–biochar mixture incubated for 4 mo at 70°C. Fourier-transform infrared spectroscopy can provide direct information about the functional groups of soil organic matter fractions (Baes and Bloom, 1989; Davis et al., 1999; Kaiser et al., 1997; Niemeyer et al., 1992). For example, FTIR spectroscopy has been used to evaluate the decomposition pathways of organic surface layers of forest soils (Haberhauer et al., 1998; Wershaw et al., 1996) and changes that occur during composting (Inbar et al., 1989). More recently, DR-FTIR (also known as DRIFT) spectroscopy in combination with multivariate data analysis has gained widespread acceptance as a rapid laboratory-or field-based method for the quantification of organic C and black carbon in soils (Bornemann et al., 2008; Reeves et al., 2008). Harvey et al. (2012) used two-dimensional perturbation based correlation infrared spectroscopy to understand the mechanisms controlling the structure–reactivity relationship in biochar produced at different temperatures. The objective of our research was to use DR-FTIR to estimate the biochar content and to observe the structural changes that occurred to biochar during mineralization in a laboratory incubation experiment (Fang et al., 2014a, 2014b).

MATERIALS AND METHODS

Soils and Biochars

Incubation experiment details and soil and biochar properties used in the study have been described elsewhere (Fang et al., 2014a, 2014b). To obtain aged biochars in soils, four soils (one each Inceptisol, Oxisol, Entisol, and Vertisol) with contrasting soil properties, including clay mineral composition, were incubated with two biochars at 2% (w/w). The two biochars were produced at 450°C (B450) and 550°C (B550) from a ^{13}C-depleted ($\text{™}^{13}C = -36‰$) woody biomass (*Eucalyptus saligna* Sm.). The soil–biochar mixtures were incubated at ~70% of water holding capacity in sealed jars at 20, 40, and 60°C. The CO_2 evolved from the mixtures was continuously trapped in 2.5 mol L^{-1} NaOH solution, and the trap solution was changed at regular intervals. The total amount of C mineralized (as CO_2) from the biochar-amended soils was determined by titrating a known aliquot of the trap solution (i.e., 2.5 mol L^{-1} NaOH) against 0.1 mol L^{-1} HCl, using phenolphthalein as the indicator. To determine the proportion of C mineralized from the biochar and soil C components, a portion of the CO_2 trap solution was mixed with $SrCl_2$ to precipitate the trapped CO_2 as $SrCO_3$; the precipitate was analyzed for $\text{™}^{13}C$ using an isotope-ratio mass spectrometer (IRMS; Delta V Thermo Finnigan) (Keith et al., 2011). The actual amount of biochar C and native soil C mineralized was then calculated from the total C mineralization data.

Density Fractionation of Biochar and Soil Carbon

The light density fraction of the soil–biochar mixtures and soils, consisting mainly of biochar C and the native soil organic fraction, was separated using a solution of 1.8 g cm^{-3} sodium polytungstate ($H_2Na_6O_{40}W_{12}$) (Golchin et al., 1994; Sohi et al., 2001). The light fraction (<1.8 g cm^{-3}) from the soil–biochar mixtures (and control soils) was recovered on Day 0 (i.e., immediately after mixing the soil and biochar) and 6 and 12 mo after incubation at the three temperatures. For isolation of the light fraction, an equal quantity of soil or soil–biochar mixture was taken from each of the four replicates as described elsewhere (Fang et

al., 2014a, 2014b). The recovery of the biochars in the light fraction was generally good for the Inceptisol, Vertisol, and Oxisol, with an average value of >80%. However, in the Entisol the recovery was very low (average = 28%) and many negative values were obtained in this soil. The presence of calcite might have contributed to the incorporation of biochar in soil microaggregates and the subsequent poor recovery of biochar in the light fraction of the Entisol. The isolated light fraction was washed thoroughly with deionized water and dried at 70°C before analysis. The light-density fraction materials were characterized for C content and mineralogy using X-ray diffraction and DR-FTIR analysis. Total C and ™^{13}C analyses were performed using the IRMS.

X-ray Diffraction Analysis

Soil samples were dispersed, and the clay fractions (<2 ∝m) were separated for the identification of clay minerals. Both oriented and random powder X-ray diffraction (XRD) patterns were obtained for the clay fraction using a GBC MMA diffractometer (35 kV and 28.5 mA) with monochromatic CuK⟨ radiation. The oriented samples were given standard pretreatments for the identification of phyllosilicate minerals (Brown and Brindley, 1980). Random powder XRD analysis was performed on finely ground clay fractions of the soils, the two original biochars, and the light-density fractions separated from the biochar-amended soils.

Fourier-Transform Infrared Spectroscopy

For the FTIR analyses, 10 mg of the isolated light fraction, consisting of biochar and soil organic matter, was mixed with 190 mg of spectroscopic-grade KBr; the mixture was first hand ground and then ground in a Wig-L-bug using a stainless steel vial with a stainless steel ball pestle for 30 s. The ground mixture was pressed into an Al holder for the analysis. The FTIR measurements were performed with a Nicolet 6700 FTIR spectrometer (Thermo Scientific) using a smart diffuse reflectance accessory (Thermo Scientific). The FTIR spectra were collected using a liquid N_2 cooled MCT (HgCdTe) detector. The scans were obtained in the range from 4000 to 650 cm^{-1} with a resolution of 4 cm^{-1} and 64 scans per sample. The spectrum of each sample was ratioed against the background spectrum obtained from the diffuse reflectance spectrum of pure KBr.

To quantify the area of the aromatic and aliphatic ν(CH) bands, the spectra were baseline corrected in the 3200 to 2700 cm^{-1} region using a quartic fitting function. The integrated area of the aromatic ν(CH) bands was determined by spectral integration of the FTIR spectra between 3150 and 3000 cm^{-1}, and the aliphatic ν(CH) bands were determined based on the area under the curve in the 3000 to 2750 cm^{-1} region.

RESULTS AND DISCUSSION

The FTIR spectra of the two fresh biochars, i.e., B450 (biochar produced at 450°C) and B550 (biochar produced at 550°C), are presented in Fig. 1, and the band positions and assignments are listed in Supplemental Table S1 based on the published literature (Cheng et al., 2006; Haberhauer et al., 1998; Morterra et al., 1984; Farmer, 1974; Tatzber et al., 2007; Wang and Johnston, 2000). X-ray diffraction patterns for the soil clay fractions and the light

fraction isolated from each soil and the original biochars are shown in Fig. 2 and 3. Both biochars showed a broad band centered at 3400 cm^{-1} (Fig. 1), which is mainly comprised of the ν(OH) of sorbed water and hydrous minerals, with smaller contributions from ν(NH). In the B550 biochar spectrum, two distinct bands at 3638 and 3055 cm^{-1} were observed. Although the origin of the 3638 cm^{-1} band is not completely understood, the position of this band is coincident with the ν(OH) bands of expandable 2:1 clay minerals; however, no such minerals were identified in the random powder XRD analysis of the biochar. The 3055 cm^{-1} band was assigned to aromatic ν(CH), and the relative intensity of this band increased with increasing pyrolysis temperature, consistent with recent literature reports (Kloss et al., 2012). Weak, poorly resolved aliphatic ν(CH) stretching bands between 2750 and 2950 cm $^{-1}$ were also present in the spectra of both biochars. In addition to the aromatic ν(CH) band at 3055 cm^{-1}, the relative intensity of the aromatic ν(C=C) band at 1594 cm^{-1} was greater in the B550 biochar than in the B450 biochar. These results are consistent with expected trends based on prior NMR and FTIR biochar characterization studies (Kloss et al., 2012; McBeath and Smernik, 2009). The bands at 1442 and 876 cm^{-1} in the B550 FTIR spectrum were assigned to calcite (Sadtler Research Laboratories, 1982) (Supplemental Table S1). The presence of calcite in the B550 sample is consistent with the XRD analysis of the biochar (Fig. 2C). The sharp bands at 1317 and 781 cm^{-1} in the low-temperature biochar (B450) were attributed to the presence of whewellite (Sadtler Research Laboratories, 1982) (see Supplemental Table S1), and the mineral was also identified from the X-ray diffraction analysis of the B450 biochar (Fig. 2C).

Supplemental Table S1 lists the band positions and assignments (if known) of the biochars and the light fraction of the four experimental soils with and without biochar amendments. The spectra of the light fractions (density <1.8 g cm^{-3}) isolated from the control (without biochar amendment) and the soils amended with the two biochars (i.e., B450 and B550) immediately after mixing (Day 0) are presented in Fig. 4. The spectra of the light fractions from the biochar-amended soils show most of the bands observed in the pure biochars. Additionally, absorption bands due to native organic matter and soil minerals were also observed. For the Vertisol, Oxisol, and Inceptisol, the addition of the biochar was clearly evidenced by the strong biochar ν(C=C) band at ~1600 cm^{-1}. However, the presence of biochar was less evident in the light fraction of the calcareous Entisol, which is consistent with the poor recovery of biochar from this soil as described above.

The Inceptisol had very low clay content (1.3%), and the clay mineralogy was dominated by kaolinite with trace amounts of quartz, hydroxy-interlayered vermiculite (HIV), and illite (Fig. 2A and 2B). The FTIR spectra of the soil and of the biochar-amended soil clearly reveal the diagnostic features of kaolinite and quartz (Fig. 4A; Supplemental Table S1). The presence of kaolinite is revealed by the ν(OH) bands at 3695, 3668, 3651, and 3620 cm^{-1}, the ν(Si–O) bands at 1108, 1033, 1011 cm^{-1}, and ™(OH) deformation bands at 937 and 914 cm^{-1}. In addition, the quartz “doublet” at 798 and 780 cm^{-1} is evident. X-ray diffraction analysis also showed the presence of kaolinite and quartz in the light-density fraction isolated from this soil (Fig. 3). The addition of the B450 and B550 biochar to the Inceptisol is clearly seen in the aromatic ν(C=C) band at ~1600 cm^{-1}. The C contents of the light fraction of the Inceptisol, Inceptisol + B450 (2%), and Inceptisol + B550 (2%) were 28.3, 39.4, and 49.9%, respectively.

X-ray diffraction profile analysis of the clay fraction of the Oxisol indicated the presence of goethite, gibbsite, kaolinite, hematite, anatase, and HIV (Fig. 2A and 2B). Consistent with the XRD data of the clay fraction (Fig. 2A and 2B) and the light-density fraction (Fig. 3), the FTIR spectra revealed the ν(OH), ν(OH), and ν(Si–O) bands of kaolinite (band positions are the same as for kaolinite features in the Inceptisol) (Fig. 4B). In addition, the bands at 3621, 3527, 3447, 3394, and 3377 cm^{-1} are all consistent with reported positions of the ν(OH) bands of gibbsite (Wang and Johnston, 2000) (Supplemental Table S1). Similar to the Inceptisol, the addition of biochar to the Oxisol is clearly evidenced in the FTIR spectra of the light fraction by the growth of the aromatic ν(C=C) band at 1600 cm^{-1}. The total C content of the light fractions of the Oxisol, Oxisol + B450 (2%), and Oxisol + B550 (2%) were 24.0, 53.4, and 59.6%, respectively.

The FTIR spectrum of the light fraction isolated from a Vertisol is shown in Fig. 4C. The dominant mineralogy of this soil is smectite, with small amounts of kaolinite (Fig. 2A and 2B). The light-density fraction isolated from the Vertisol shows all the minerals (i.e., smectite, kaolinite, quartz, and feldspar) that were identified in the clay fraction of this soil (Fig. 3). The FTIR spectrum reveals only features consistent with the presence of smectite, with a broad ν(OH) feature at 3621 cm^{-1} (structural OH), ν(Si–O) bands at 1091 and 1025 cm^{-1}, and OH deformation (bending) bands at 913 and 875 cm^{-1} assigned as Al–O(H)– Al, and Al–O(H)–Fe modes, respectively (Farmer, 1974; Xu et al., 2000). The presence of sorbed water is also evidenced by the strong broad feature at 3400 cm^{-1} and in the H–O–H bending region near 1640 cm^{-1}. Similar to the Inceptisol and Oxisol, the addition of biochar is clearly evident in the FTIR spectra of the light fractions of the Vertisol. The total C content of the light fractions of the Vertisol, Vertisol + B450, and Vertisol + B550 were 29.2, 52.9, and 58.5%, respectively.

The FTIR spectrum of the light fraction of the calcareous Entisol is shown in Fig. 4D and Supplemental Table S1. Unlike the other three soils, this soil did not clearly reflect the addition of the biochar with a little change in the area of the intensity in the biochar ν(C=C) region around 1600 cm^{-1}. The strongest band present in three spectra is the carbonate band at 1452 cm^{-1}. Illite has a strong ν(Si–O) band at 1030 cm^{-1} but is relatively featureless in the ν(OH) region. The presence of illite and calcite is consistent with the XRD results of the light fraction of the soil (Fig. 3). Similar to the other soils, all minerals (illite, kaolinite, calcite, and feldspar) identified in the clay fraction of the Entisol (Fig. 2A and 2B) were also found in the light-density isolates of the soil (Fig. 3). The limited recovery of the applied biochars and the lack of biochar in the light fraction of this soil is also reflected in the largely similar total C content of the light fractions of the Entisol, Entisol + B450, and Entisol + B550, with values of 30.7, 31.4, and 36.1%, respectively.

Relationship of Aromatic/Aliphatic Ratio with Biochar Mineralization in Soil

As the spectra in Fig. 4 illustrate, the biochar absorption bands overlap with those of the native soil organic C. In addition, the mineralogy of the four soils is strongly contrasting, and, in some cases, the vibrational bands of the minerals and the bound water associated with these minerals interfere with the analysis of the biochar bands. To assess the structural stability of biochar as a function of time and temperature of incubation, we analyzed the

ν(CH) region of the light fractions isolated from four soils (control and biochar-amended soils) in detail. In particular, we were interested in the change in the aromatic to aliphatic character of the native soil organic C and biochar C. Although biochar is generally regarded as a stable, recalcitrant material, depending on the pyrolysis temperature these materials contain variable amounts of labile C, which is mainly aliphatic in character (Harvey et al., 2012; McBeath and Smernik, 2009). To assess structural changes of the biochar, we analyzed the ν(CH) region of the four soils and amended soils to derive a ratio of the C–H stretching of aromatic groups at 3050 cm^{-1} to the area of C–H stretching bands of aliphatic groups between 2950 and 2750 cm^{-1}. This is illustrated in Fig. 5 with an expanded plot of the original Inceptisol in the ν(CH) region. The spectra were baseline corrected, and the integrated areas of the aromatic ν(CH) bands (3150–3030 cm^{-1}) and the alkyl ν(CH) bands (3030–2750 cm^{-1}) were determined for all soils. Although these bands are free from interference from the other mineral phases present in the samples, the spectra in this region contain contributions from both the biochar and the native soil organic C present. The integrated area of these bands was determined after background correction, and the peak area ratio of aromatic to aliphatic bands (Ar/Al) was calculated.

The Ar/Al ratios of the light C fraction isolated from the control and biochar-amended soils were plotted against the amount of biochar C mineralized from the soils after 6 and 12 mo of incubation (Fig. 6). For the B550-amended soils, the Ar/Al ratio of the light fractions increased systematically with biochar application, temperature, and time of incubation compared with the control soils (Fig. 6; Supplemental Table S2). However, this trend was not evident for the B450-amended soils with the exception of the Entisol. The Ar/Al ratio in the case of B550 was highly positively and linearly correlated with the amount of biochar C mineralized after 6 and 12 mo of aging in all soils; the correlation was relatively poor in the Oxisol due to the presence of an outlier. Moreover, the Oxisol had the greatest stabilization effect on biochar C mineralization, i.e., the minimum amount of biochar C was mineralized in this soil (Fang et al., 2014a, 2014b), and this may have contributed to the weaker relationship observed for the soil.

The Ar/Al ratio was greater for the light fraction from the B550-amended soils than from the corresponding fractions from the B450-amended soils. These results suggest the presence of a greater proportion of labile C in the lower temperature biochar (B450) than in the higher temperature biochar (B550), consistent with the spectroscopic data for the original biochars shown in Fig. 1 and prior studies (Harvey et al., 2012; Krull et al., 2003; McBeath and Smernik, 2009). The mineralization data from the incubation study related to these samples show that approximately twice as much C was mineralized from the B450-amended soils than from the B550-amended soils (Fang et al., 2014a, 2014b).

Unlike ^{13}C NMR-based analyses of aliphatic to aromatic functional groups of soil organic C, this FTIR ratio is based on the relative C–H content among aromatic and aliphatic groups. It should be pointed out that the area of the aromatic ν(CH) band *underestimates* the amount of aromatic C present, the H content of alkyl C chains is 16.3% compared with 7.7% for a simple benzene ring, and further aromatic ring condensation results in progressively lower H contents (e.g., naphthalene has a H content of 6.3% while that of pyrene is 5.5%). Thus, the Ar/Al ratio determined in this study underestimated the amount of aromatic C present.

The results for the limited biochar samples incubated in four soils suggest that the Ar/Al ratio determined by FTIR can be a sensitive measure of changes in the aromatic and aliphatic forms of C and the extent of biochar C mineralization in a variety of biochar-amended soils. Diffuse reflectance FTIR spectroscopy also revealed that the ratio of the aromatic (3050 cm^{-1}) to aliphatic (2950–2750 cm^{-1}) in the light fraction of the soils incubated with two different biochars systematically changed as a function of the type of biochar, time of incubation, temperature of incubation, and type of soil. A linear correlation existed between the Ar/Al ratios for the light fraction (<1.8 g cm^{-3}) isolated from B550-amended soils and the biochar C mineralized from these soils; these relationships were unique for each soil type, indicating that the ratio is affected by the composition of native soil organic C, interactive priming of native soil C and biochar C, and the interaction of biochar with the native soil organic C and mineral fraction in the soil. A similar linear correlation also existed between the Ar/Al ratios for the light fraction (<1.8 g cm^{-3}) isolated from B550-amended soils and the native soil C mineralized from these soils (Supplemental Fig. S1). However, such relationships were not observed for the B450-amended soils that contained a substantially larger proportion of aliphatic C than the B550-amended soils. The results indicate that DR-FTIR offers a simple procedure for long-term monitoring of biochars pyrolyzed at higher temperatures. Further research is, however, required for developing a similar method for biochars containing high amounts of labile aliphatic C, and the combination of thermogravimetric analysis and DR-FTIR may prove useful in such cases.

CONCLUSIONS

In this study, a spectroscopic index derived from aromatic (3050 cm^{-1}) and aliphatic (2950–2750 cm^{-1}) bands was developed to monitor changes in biochar C with aging in soil. A linear correlation existed between the Ar/Al ratios for the light fraction (<1.8 g cm^{-3}) isolated from B550-amended soils and the biochar C mineralized from these soils; these relationships were unique for each soil type. However, such relationships were not observed for the B450-amended soils, which contained a substantially larger proportion of aliphatic C than the B550 biochar. The results indicate that DR-FTIR offers a simple procedure for long-term monitoring of biochars pyrolyzed at higher temperatures. Further research is, however, required for developing a similar method for biochars containing high amounts of labile aliphatic C.

Supplementary Material

Refer to Web version on PubMed Central for supplementary material.

Acknowledgments

We would like to thank Gnanashiri S. Premachandra for his help in the DR-FTIR analysis and Bhupinderpal Singh from NSW DPI and Evelyn Krull from CSIRO Land and Water for their input in devising the soil–biochar incubation experiments. We acknowledge financial support from the Australian Government under its Climate Change Research Program and the University of Sydney.

Abbreviations

DR-FTIR	diffuse reflectance Fourier-transform infrared
FTIR	Fourier-transform infrared
NMR	nuclear magnetic resonance
XRD	X-ray diffraction

References

Baes AU, Bloom PR. Diffuse reflectance and transmission Fourier transform infrared (DRIFT) spectroscopy of humic and fulvic acids. Soil Sci Soc Am J. 1989; 53:695–700. DOI: 10.2136/sssaj1989.03615995005300030008

Baldock JA, Oades JM, Nelson PN, Skene TM, Golchin A, Clarke P. Assessing the extent of decomposition of natural organic materials using solid-state ^{13}C NMR spectroscopy. Aust J Soil Res. 1997; 35:1061–1083. DOI: 10.1071/S97004

Baldock JA, Smernik RJ. Chemical composition and bioavailability of thermally altered *Pinus resinosa* (red pine) wood. Org Geochem. 2002; 33:1093–1109. DOI: 10.1016/S0146-6380(02)00062-1

Bornemann L, Welp G, Brodowski S, Rodionov A, Amelung W. Rapid assessment of black carbon in soil organic matter using mid-infrared spectroscopy. Org Geochem. 2008; 39:1537–1544. DOI: 10.1016/j.orggeochem.2008.07.012

Brodowski S, Amelung W, Haumaier L, Abetz C, Zech W. Morphological and chemical properties of black carbon in physical soil fractions as revealed by scanning electron microscopy and energy-dispersive X-ray spectroscopy. Geoderma. 2005a; 128:116–129. DOI: 10.1016/j.geoderma.2004.12.019

Brodowski S, Rodionov A, Haumaier L, Glaser B, Amelung W. Revised black carbon assessment using benzene polycarboxylic acids. Org Geochem. 2005b; 36:1299–1310. DOI: 10.1016/j.orggeochem.2005.03.011

Brown, G., Brindley, GW. X-ray diffraction procedures for clay mineral identification. In: Brindley, GW., Brown, G., editors. Crystal structures of clay minerals and their X-ray identification. Mineral Soc; London: 1980. p. 305-359.

Cheng CH, Lehmann J, Engelhard MH. Natural oxidation of black carbon in soils: Changes in molecular form and surface charge along a climosequence. Geochim Cosmochim Acta. 2008; 72:1598–1610. DOI: 10.1016/j.gca.2008.01.010

Cheng CH, Lehmann J, Thies JE, Burton SD, Engelhard MH. Oxidation of black carbon by biotic and abiotic processes. Org Geochem. 2006; 37:1477–1488. DOI: 10.1016/j.orggeochem.2006.06.022

Davis WM, Erickson C, Johnston CT, Delfino JJ, Porter JE. Quantitative Fourier transform infrared spectroscopic investigation of humic substance functional group composition. Chemosphere. 1999; 38:2913–2928. DOI: 10.1016/S0045-6535(98)00486-X

Fang Y, Singh B, Singh BP, Krull E. Biochar carbon stability in four contrasting soils. Eur J Soil Sci. 2014a; 65:60–71. DOI: 10.1111/ejss.12094

Fang Y, Singh BP, Singh B. Temperature sensitivity of biochar and native carbon mineralization in biochar-amended soils. Agric Ecosyst Environ. 2014b; 191:158–167. DOI: 10.1016/j.agee.2014.02.018

Farmer, VC. The layer silicates. In: Farmer, VC., editor. The infrared spectra of minerals. Mineral Soc; London: 1974. p. 331-359.

Fuertes AB, Arbestain MC, Sevilla M, Macia-Agullo JA, Fiol S, Lopez R, et al. Chemical and structural properties of carbonaceous products obtained by pyrolysis and hydrothermal carbonisation of corn stover. Aust J Soil Res. 2010; 48:618–626. DOI: 10.1071/SR10010

Gaskin JW, Steiner C, Harris K, Das KC, Bibens B. Effect of low-temperature pyrolysis conditions on biochar for agricultural use. Trans ASAE. 2008; 51:2061–2069. DOI: 10.13031/2013.25409

Glaser B, Balashov E, Haumaier L, Guggenberger G, Zech W. Black carbon in density fractions of anthropogenic soils of the Brazilian Amazon region. Org Geochem. 2000; 31:669–678. DOI: 10.1016/S0146-6380(00)00044-9

Glaser B, Lehmann J, Zech W. Ameliorating physical and chemical properties of highly weathered soils in the tropics with charcoal: A review. Biol Fertil Soils. 2002; 35:219–230. DOI: 10.1007/s00374-002-0466-4

Golchin A, Oades JM, Skjemstad JO, Clarke P. Soil structure and carbon cycling. Aust J Soil Res. 1994; 32:1043–1068. DOI: 10.1071/SR9941043

Haberhauer G, Rafferty B, Strebl F, Gerzabek MH. Comparison of the composition of forest soil litter derived from three different sites at various decompositional stages using FTIR spectroscopy. Geoderma. 1998; 83:331–342. DOI: 10.1016/S0016-7061(98)00008-1

Harvey OR, Herbert BE, Kuo LJ, Louchouarn P. Generalized two-dimensional perturbation correlation infrared spectroscopy reveals mechanisms for the development of surface charge and recalcitrance in plant-derived biochars. Environ Sci Technol. 2012; 46:10641–10650. DOI: 10.1021/es302971d [PubMed: 22950676]

Hedges JI, Eglinton G, Hatcher PG, Kirchman DL, Arnosti C, Derenne S, et al. The molecularly-uncharacterized component of nonliving organic matter in natural environments. Org Geochem. 2000; 31:945–958. DOI: 10.1016/S0146-6380(00)00096-6

Hilscher A, Knicker H. Carbon and nitrogen degradation on molecular scale of grass-derived pyrogenic organic material during 28 months of incubation in soil. Soil Biol Biochem. 2011; 43:261–270. DOI: 10.1016/j.soilbio.2010.10.007

Inbar Y, Chen Y, Hadar Y. Solid-state carbon-13 nuclear magnetic resonance and infrared spectroscopy of composted organic matter. Soil Sci Soc Am J. 1989; 53:1695–1701. DOI: 10.2136/sssaj1989.03615995005300060014x

Kaiser K, Guggenberger G, Haumaier L, Zech W. Dissolved organic matter sorption on subsoils and minerals studied by ^{13}C NMR and DRIFT spectroscopy. Eur J Soil Sci. 1997; 48:301–310. DOI: 10.1111/j.1365-2389.1997.tb00550.x

Keith A, Singh B, Singh BP. Interactive priming of biochar and labile organic matter mineralization in a smectite-rich soil. Environ Sci Technol. 2011; 45:9611–9618. DOI: 10.1021/es202186j [PubMed: 21950729]

Kloss S, Zehetner F, Dellantonio A, Hamid R, Ottner F, Liedtke V, et al. Characterization of slow pyrolysis biochars: Effects of feedstocks and pyrolysis temperature on biochar properties. J Environ Qual. 2012; 41:990–1000. DOI: 10.2134/jeq2011.0070 [PubMed: 22751041]

Kookana RS, Sarmah AK, van Zwieten L, Krull E, Singh B. Biochar application to soil: Agronomic and environmental benefits and unintended consequences. Adv Agron. 2011; 112:103–143. DOI: 10.1016/B978-0-12-385538-1.00003-2

Krull ES, Skjemstad JO, Graetz D, Grice K, Dunning W, Cook G, Parr JF. ^{13}C-depleted charcoal from C4 grasses and the role of occluded carbon in phytoliths. Org Geochem. 2003; 34:1337–1352. DOI: 10.1016/S0146-6380(03)00100-1

Kuzyakov Y, Subbotina I, Chen HQ, Bogomolova I, Xu XL. Black carbon decomposition and incorporation into soil microbial biomass estimated by ^{14}C labeling. Soil Biol Biochem. 2009; 41:210–219. DOI: 10.1016/j.soilbio.2008.10.016

Laird DA, Chappell MA, Martens DA, Wershaw RL, Thompson M. Distinguishing black carbon from biogenic humic substances in soil clay fractions. Geoderma. 2008; 143:115–122. DOI: 10.1016/j.geoderma.2007.10.025

Lehmann J. A handful of carbon. Nature. 2007; 447:143–144. DOI: 10.1038/447143a [PubMed: 17495905]

McBeath AV, Smernik RJ. Variation in the degree of aromatic condensation of chars. Org Geochem. 2009; 40:1161–1168. DOI: 10.1016/j.orggeochem.2009.09.006

Mikutta R, Schaumann GE, Gildemeister D, Bonneville S, Kramer MG, Chorover J, et al. Biogeochemistry of mineral–organic associations across a long-term mineralogical soil gradient (0.3–4100 kyr), Hawaiian Islands. Geochim Cosmochim Acta. 2009; 73:2034–2060. DOI: 10.1016/j.gca.2008.12.028

Morterra C, Mirra C, Borello E. IR spectroscopic study of pyridine adsorption onto a-FeOOH (goethite). Mater Chem Phys. 1984; 10:139–154. DOI: 10.1016/0254-0584(84)90043-9

Namgay T, Singh B, Singh BP. Influence of biochar application to soil on the availability of As, Cd, Cu, Pb, and Zn to maize (*Zea mays* L.). Aust J Soil Res. 2010; 48:638–647. DOI: 10.1071/SR10049

Nguyen BT, Lehmann J. Black carbon decomposition under varying water regimes. Org Geochem. 2009; 40:846–853. DOI: 10.1016/j.orggeochem.2009.05.004

Nguyen BT, Lehmann J, Hockaday WC, Joseph S, Masiello CA. Temperature sensitivity of black carbon decomposition and oxidation. Environ Sci Technol. 2010; 44:3324–3331. DOI: 10.1021/es903016y [PubMed: 20384335]

Niemeyer J, Chen Y, Bollag JM. Characterization of humic acids, composts and peat by diffuse reflectance Fourier-transform infrared spectroscopy. Soil Sci Soc Am J. 1992; 56:135–140. DOI: 10.2136/sssaj1992.03615995005600010021x

Preston CM, Schmidt MWI. Black (pyrogenic) carbon: A synthesis of current knowledge and uncertainties with special consideration of boreal regions. Biogeosciences. 2006; 3:397–420. DOI: 10.5194/bg-3-397-2006

Reeves JB, McCarty GW, Rutherford DW, Wershaw RL. Mid-infrared diffuse reflectance spectroscopic examination of charred pine wood, bark, cellulose, and lignin: Implications for the quantitative determination of charcoal in soils. Appl Spectrosc. 2008; 62:182–189. [PubMed: 18284794]

Rumpel C, Janik LJ, Skjemstad JO, Kogel-Knabner I. Quantification of carbon derived from lignite in soils using mid-infrared spectroscopy and partial least squares. Org Geochem. 2001; 32:831–839. DOI: 10.1016/S0146-6380(01)00029-8

Sadtler Research Laboratories. The Sadtler infrared spectra handbook of minerals and clays. Sadtler Res. Lab.; Philadelphia, PA: 1982.

Schmidt MWI, Noack AG. Black carbon in soils and sediments: Analysis, distribution, implications, and current challenges. Global Biogeochem Cycles. 2000; 14:777–793. DOI: 10.1029/1999GB001208

Schmidt MWI, Skjemstad JO, Czimczik CI, Glaser B, Prentice KM, Gelinas Y, Kuhlbusch TAJ. Comparative analysis of black carbon in soils. Global Biogeochem Cycles. 2001; 15:163–167. DOI: 10.1029/2000GB001284

Schmidt MWI, Skjemstad JO, Jager C. Carbon isotope geochemistry and nanomorphology of soil black carbon: Black chernozemic soils in central Europe originate from ancient biomass burning. Global Biogeochem Cycles. 2002; 16(4):1123.doi: 10.1029/2002GB001939

Singh B, Singh BP, Cowie AL. Characterisation and evaluation of biochars for their application as a soil amendment. Aust J Soil Res. 2010a; 48:516–525. DOI: 10.1071/SR10058

Singh BP, Hatton BJ, Singh B, Cowie AL, Kathuria A. Influence of biochars on nitrous oxide emission and nitrogen leaching from two contrasting soils. J Environ Qual. 2010b; 39:1224–1235. DOI: 10.2134/jeq2009.0138 [PubMed: 20830910]

Skjemstad JO, Reicosky DC, Wilts AR, McGowan JA. Charcoal carbon in US agricultural soils. Soil Sci Soc Am J. 2002; 66:1249–1255. DOI: 10.2136/sssaj2002.1249

Sohi SP, Mahieu N, Arah JRM, Powlson DS, Madari B, Gaunt JL. A procedure for isolating soil organic matter fractions suitable for modeling. Soil Sci Soc Am J. 2001; 65:1121–1128. DOI: 10.2136/sssaj2001.6541121x

Tatzber M, Stemmer M, Splegel H, Katziberger C, Haberhauer G, Mentler A, Gerzabek MH. FTIR-spectroscopic characterization of humic acids and humin fractions obtained by advanced NaOH, $Na_4P_2O_7$, and Na_2CO_3 extraction procedures. J Plant Nutr Soil Sci. 2007; 170:522–529.

Wang SL, Johnston CT. Assignment of the structural OH stretching bands of gibbsite. Am Mineral. 2000; 85:739–744. DOI: 10.2138/am-2000-5-612

Wershaw RL, Leenheer JA, Kennedy KR, Noyes TI. Use of ^{13}C NMR and FTIR for elucidation of degradation pathways during natural litter decomposition and composting: 1. Early stage leaf degradation. Soil Sci. 1996; 161:667–679. DOI: 10.1097/00010694-199610000-00004

Xu W, Johnston CT, Parker P, Agnew SF. Infrared study of water sorption on Na-, Li-, Ca- and Mg-exchanged (SWy-1 and SAz-1) montmorillonite. Clays Clay Miner. 2000; 48:120–131. DOI: 10.1346/CCMN.2000.0480115

Zimmerman AR. Abiotic and microbial oxidation of laboratory-produced black carbon (biochar). Environ Sci Technol. 2010; 44:1295–1301. DOI: 10.1021/es903140c [PubMed: 20085259]

Core Ideas

- Aged biochars in different soils were analyzed using DR-FTIR in this study.
- Native soil organic C, biochar C, and minerals created distinct absorption bands.
- Ar/Al band ratio systematically changed in soils with high-temperature biochar.
- Ar/Al ratios and biochar C mineralized in the soils were linearly correlated.
- DR-FTIR is a simple procedure for long-term monitoring of high-temperature biochars.

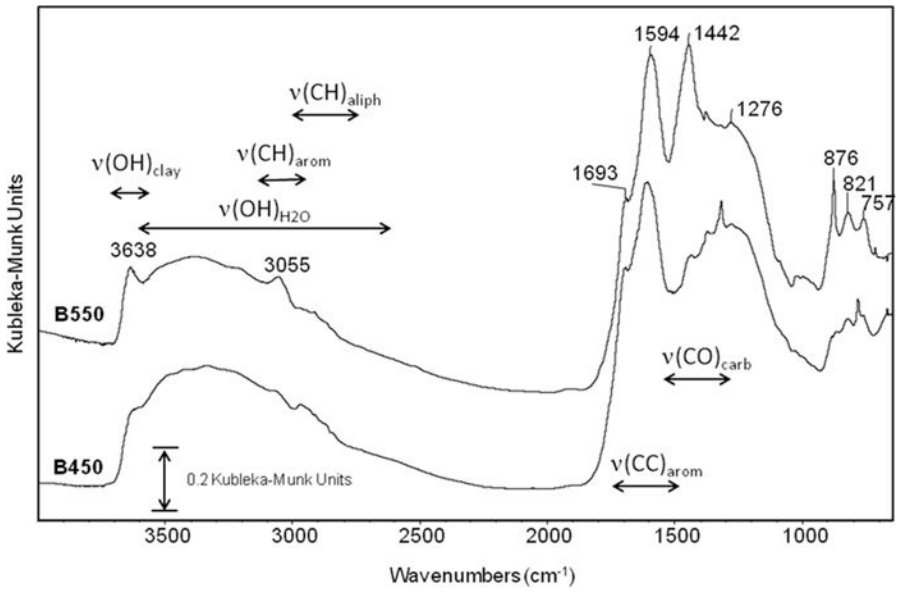

Fig. 1.

Fourier-transform infrared spectra of the two biochars in the fresh state, i.e., before addition to the soils: B450 and B550 biochars were produced at 450 and 550°C, respectively.

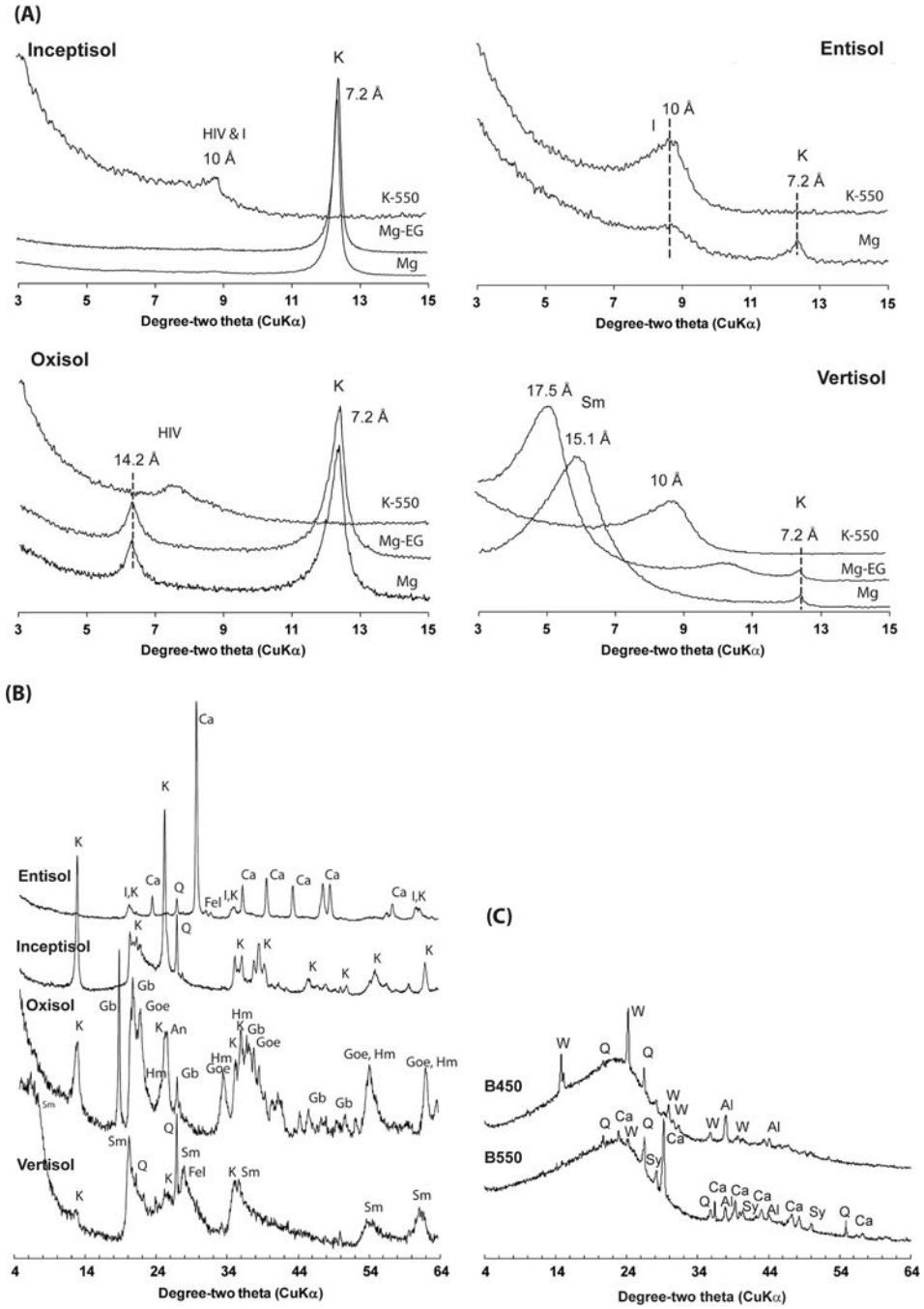

Fig. 2.

(a) X-ray diffraction patterns of the basally oriented clay fraction of the four soils after treatment: Mg saturated and air dried (Mg); Mg saturated and ethylene glycolated (Mg-EG), and K saturated and heated to 550°C (K-550); (b) random powder X-ray diffraction patterns of the four soils; and (c) random powder X-ray diffractions of the fresh biochar samples produced at 450°C (B450) and 550°C (B550). Identified peaks include hydroxy-interlayered vermiculite (HIV), illite (I), kaolinite (K), smectite (Sm), calcite (Ca), quartz (Q), feldspar (Fel), gibbsite (Gb), goethite (Goe), hematite (Hm), whewellite (W) and sylvite (Sy); Al

represents Al peaks from the sample holder (and not the samples) that was used for the analysis.

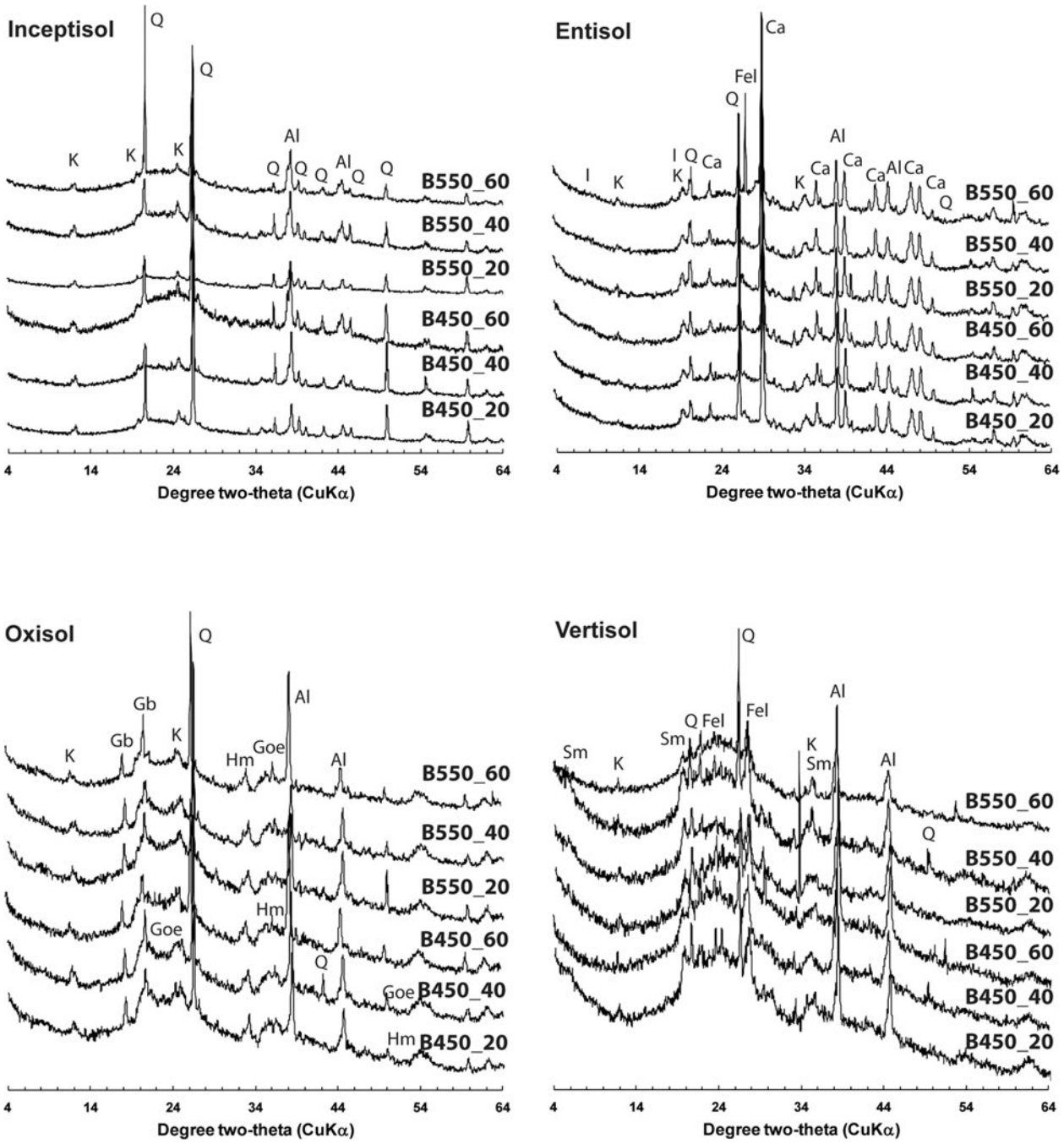

Fig. 3.

Random powder X-ray diffraction patterns of the light-density fraction (<1.8 g cm^{-3}) isolated from four soils amended with biochar produced at 450°C (B450) and 550°C (B550) and incubated at 20, 40, or 60°C for 12 mo. Identified peaks include kaolinite (K), quartz (Q), gibbsite (Gb), goethite (Goe), hematite (Hm), illite (I), calcite (Ca), feldspar (Fel), and smectite (Sm); Al represents Al peaks from the sample holder (and not the samples) that was used for the analysis.

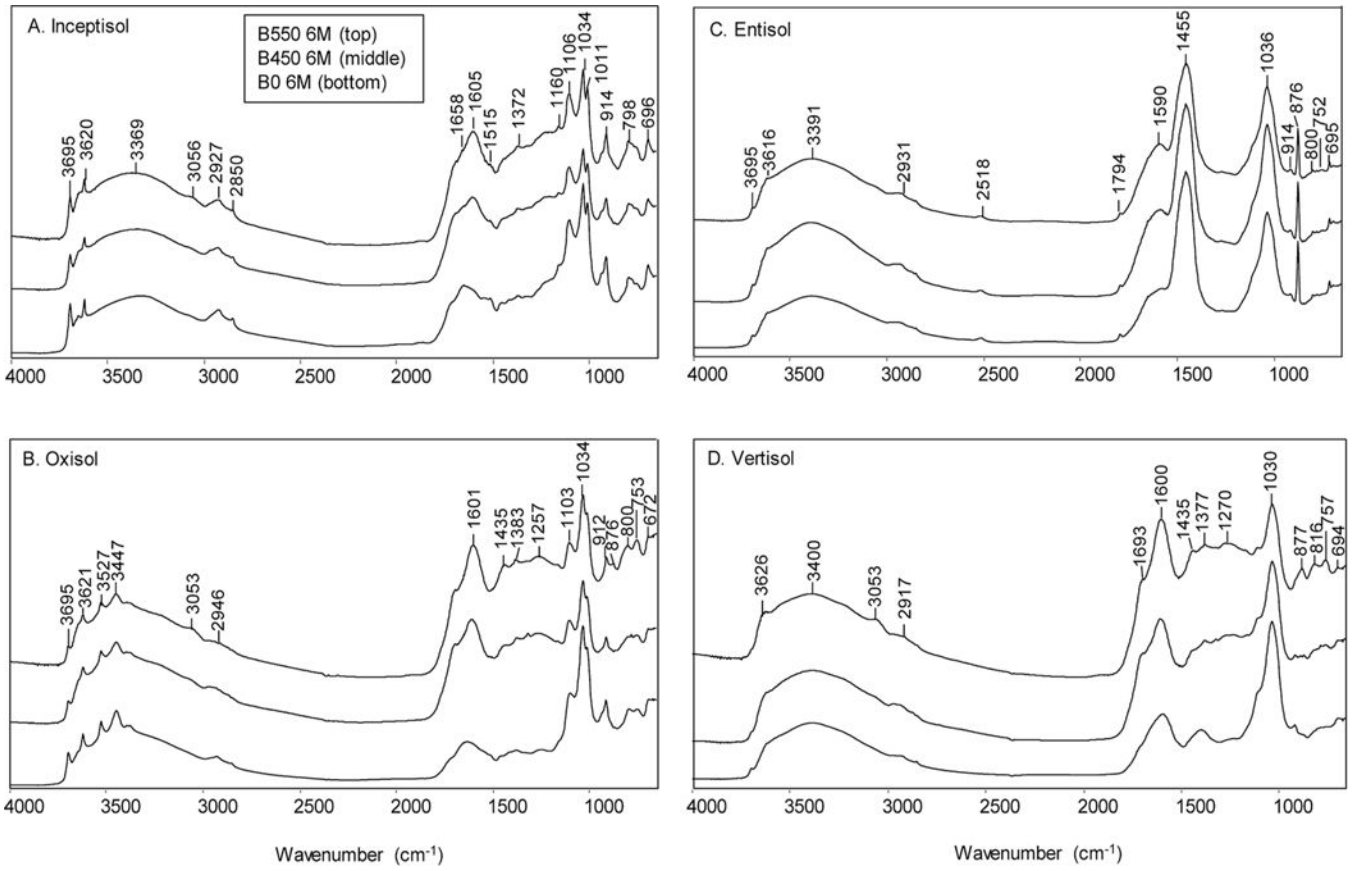

Fig. 4.

Fourier-transform infrared spectra of the light fractions (density <1.8 g cm^{-3}) of the control soils and the soil samples amended with biochars produced at 450°C (B450) and 550°C (B550) after aging 6 mo (6M) in different soils. For each of the four soils, the original soil without biochar after 6 mo aging (B0) is plotted on the bottom, the soil amended with B450 biochar is shown in the middle, and the soil amended with B550 biochar is plotted at the top.

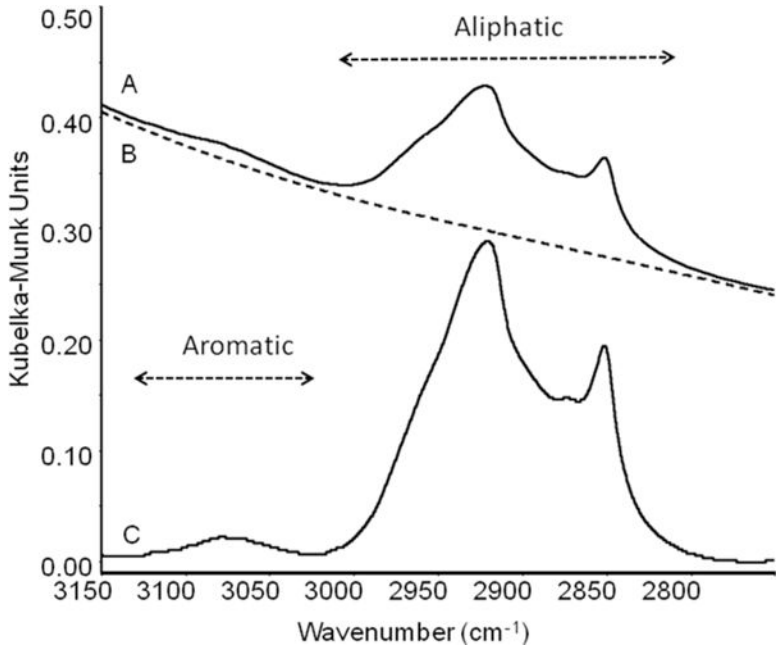

Fig. 5.

Diffuse reflectance Fourier-transform infrared spectrum of the Inceptisol soil without biochar addition at the beginning of the experiment (D0). Spectrum A corresponds to the original spectrum, Spectrum B is the baseline used to correct Spectrum A, calculated using a quartic polynomial function to correct the spectrum with *x* axis points (3227, 3212, 3184, 3154, 3132, 3006, 2796, 2785, 2768, 2749, 2695, and 2655). Spectrum C is the resulting baseline-corrected spectrum (expanded 2×). The aromatic and aliphatic regions are indicated, and the areas of these two regions represent the Ar/Al ratio.

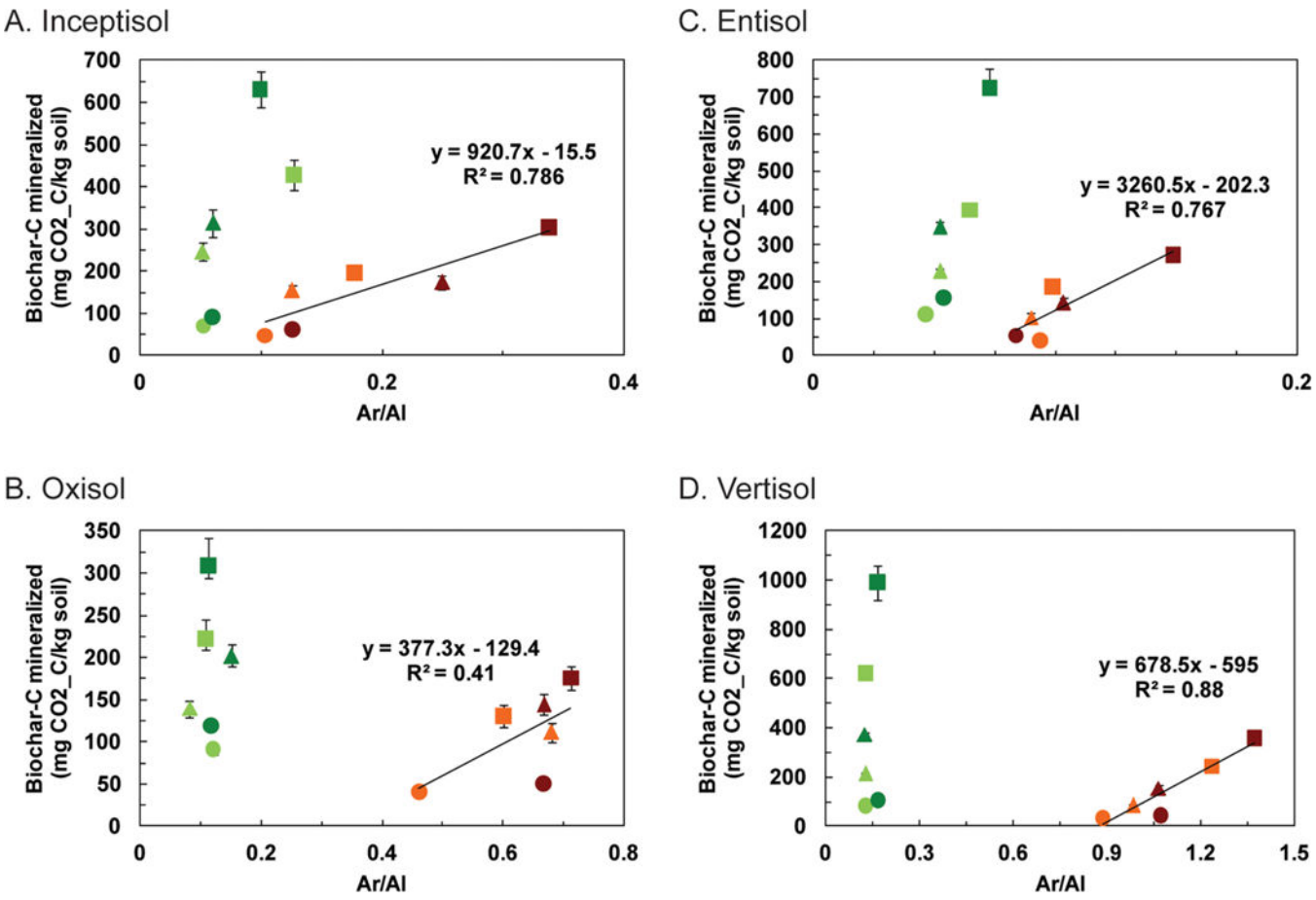

Fig. 6.

The cumulative amount of biochar C mineralized from soil–biochar mixtures after 6 (light colors) and 12 mo (dark colors) of incubation at 20 (●), 40 (▲), and 60°C (■) plotted against the aromatic/aliphatic (Ar/Al) ratio of the light fraction for the four soils. Biochars were produced at 450°C (B450, green) and 550°C (B550, brown). Error bars represent standard errors of the mean biochar C mineralized (n = 4).